XVIII[èmes] Journées Nationales Génie Côtier – Génie Civil
Anglet, 2024
DOI:10.5150/jngcgc.2024.018 *© Editions Paralia CFL*
disponible en ligne – http://www.paralia.fr – available online

Numerical study of infragravity waves dynamics with a phase-resolving model – Site of Grande Plage of Biarritz

Jonas PINAULT [1,2], Denis MORICHON [1], Matthias DELPEY [3], Volker ROEBER [1]

1. Université de Pau et des Pays de l'Adour, E2S-UPPA, SIAME, Anglet, 64600, France. *jonas.pinault@wm-consultants.fr*
2. SAS WAELES MARINE CONSULTANTS, 53 rue du Commandant Groix, 29200 Brest, France
3. SUEZ Eau France, Rivages Pro Tech, Bidart, 64210, France

Abstract:
Infragravity (IG) waves are low-frequency waves generated by energy transfers from gravity waves mostly in the nearshore area. Recent studies have shown the importance of those long waves in nearshore processes with direct implications especially in sediment transport and wave runup. Consequently, IG waves can influence two main coastal risks threatening human activities, namely erosion and coastal flooding. In this work, the behavior of infragravity waves in storm conditions on the Grande Plage of Biarritz, a mesotidal embayed beach in SW of France, is investigated using a Boussinesq-type wave model validated with field observations. At the peak of the studied storm, large IG waves were observed, with significant height up to 1 m, which are well captured by the model. A spectral analysis reveals a nodal structure in the infragravity band under certain conditions, which is characteristic of reflective beaches, where waves are not fully dissipated and reflect at the shoreline. Further analysis of the IG waves near the shoreline showed that the dissipation of the IG wave energy is highly modulated by the tide, which might result from the interactions of the IG-waves with the different slopes of the beach profile depending on the tidal level and indicates wave breaking as the main dissipation mechanism of IG wave energy. Furthermore, the relationship between the IG waves and the IG swash is found frequency-dependent, with the longest waves generating the highest swash. The reflected IG waves signal was found to correlate better with the IG swash than the incident signal due to dissipation occurring prior to the swash zone.

Keywords:
Infragravity waves, Hydrodynamics, Phase-resolving model, Wave runup, Swash, Boussinesq model.

1. Introduction

Infragravity (IG) waves are low-frequency surface ocean waves with periods typically ranging from 20 s up to 300 s or more. These long waves are related to the presence of groups in the incident short gravity waves (SW). While their heights in deep-water are relatively small (less than a few centimeters), they can grow up to more than 1 m at the shoreline, especially under storm conditions (BERTIN *et al.,* 2020). Many studies have highlighted the pivotal role of IG waves in nearshore processes, influencing especially sediment transport and wave runup, posing significant challenges for coastal communities and infrastructures. Owing to their large wavelengths, IG waves will not necessarily break and dissipate entirely their energy in shallow water, as opposed to shorter gravity waves. Hence, the remaining energy will reflect at the shoreline and propagate back seaward (DE BAKKER *et al.,* 2014). The total or partial dissipation of IG waves in the nearshore area is generally due to bottom friction, energy transfers back to the SW frequency band, or IG wave breaking (VAN DONGEREN *et al.,* 2007). On gently sloping sandy beaches, several studies have proposed IG wave breaking as the main dissipation mechanism (DE BAKKER *et al,* 2014; INCH *et al.,* 2017; BERTIN *et al*., 2020), while also highlighting the important effect of the tidal modulation to this mechanism. In the present work, the dynamics of IG waves are investigated on an intermediate reflective beach based on numerical computations from a Boussinesq-type model.

2. Methodology

2.1 Study site

The Grande Plage of Biarritz (GPB) is a 600 m long engineered beach within a 1.2 km long embayment located in the South-West of France (Figure 1 (a)). GPB opens to the Bay of Biscay and is mainly exposed to sea swells approaching from the WNW direction (around 315°). Its orientation and relatively low altitude make it vulnerable to storm impact, with overtopping events regularly observed during the winter season (Figure 1 (b)).

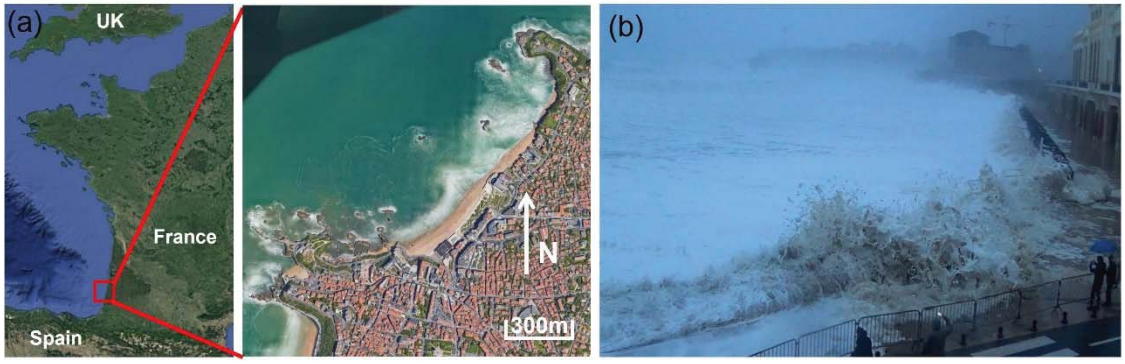

Figure 1. Location and situation of the study site: the Grande Plage of Biarritz (GPB). (a) Location of the GPB. (b) Illustration of a wave overtopping event during the Ciara storm in February 2020 (Credit : SurfingBiarritz).

The morphology of the beach is characterized by a low-sloping zone (β~2-3%) in the subtidal zone up to the lowest part of the intertidal zone, while the foreshore is quite steep (β~8-10%). For that reason, the GPB is characterized as intermediate-reflective beach (MORICHON *et al.,* 2018).

2.2 Numerical wave model

The phase-resolving, Boussinesq-type model *BOSZ* (ROEBER *et al.*, 2010; ROEBER & CHEUNG, 2012) is used to compute the hydrodynamics of the surf and swash zones. The computational domain extends 2.5 km offshore (up to the 18 m isobath) and spans 3.5 km in the longshore direction. A uniform grid size of 3.5 m by 3.5 m is used, as a reasonable compromise between numerical accuracy, stability, and computational cost for the assessment of the beach hydrodynamics, as detailed in PINAULT *et al.,* (2020). The model is run for 1.5 h where the data from the last hour is analyzed. In the present work, the analysis is focused on one cross-shore transect extracted from the 2D results (black line on Figure 2 (a)). A more detailed description of the model set-up is provided in PINAULT *et al.,* (2022).

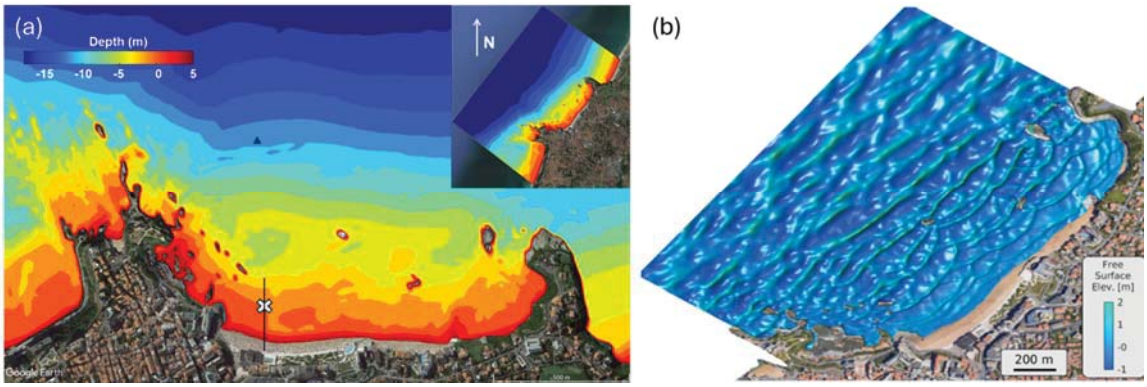

Figure 2. (a) Bathymetry of the GPB with the cross-shore transect analyzed in this study (black line) and pressure sensor location (white cross). (b) Free surface output around the area of interest produced by the numerical model.

2.3 Model output processing

The frequency components, respectively IG (0.003-0.05~Hz) and SW (0.05-0.25~Hz), of the significant wave and swash heights are calculated respectively as follows:

$$H_{IG/SW}, S_{IG/SW} = 4\sqrt{\int_{f_1}^{f_2} E(f)\,\mathrm{df}} \qquad (1)$$

where E(f) is the PSD value at the frequency *f* of either the free surface or the swash elevation time series. The incident and reflected wave spectra are computed using collocated free surface elevation and horizontal velocity (SHEREMET *et al*., 2002):

$$E^{\pm}(f) = \frac{1}{4}\left[Co_{\eta\eta}(f) + \frac{h}{g}Co_{uu}(f) \pm \left(2\sqrt{\frac{h}{g}}Co_{\eta u}(f)\right)\right] \quad (2)$$

where $Co_{\eta\eta}$ and Co_{uu} are the autospectra of the free surface elevation η and the horizontal velocity u respectively, and $Co_{\eta u}$ is the η − u cospectrum.
The reflection coefficient R^2, characterizing the amount of energy that is being reflected at the shoreline, is computed as:

$$R^2 = \frac{\int_{f_1}^{f_2} E^-(f)}{\int_{f_1}^{f_2} E^+(f)} \quad (3)$$

2.4 Model validation

This study focuses on a 3-day storm event from 31/01/2018 to 02/02/2018 when field data were collected. Offshore wave conditions ranged from moderately energetic ((Hs, Tp)=(1.5 m, 11 s)) to storm conditions with values reaching (Hs, Tp)=(4.5 m, 14 s) (Figure 3 (a)), with a mean direction of 315°. To analyze the data, the conditions have been attributed to different classes, depending on the tidal level (low, mid, and high tide, in color on Figure 3 (a)) and wave conditions (moderate to energetic).

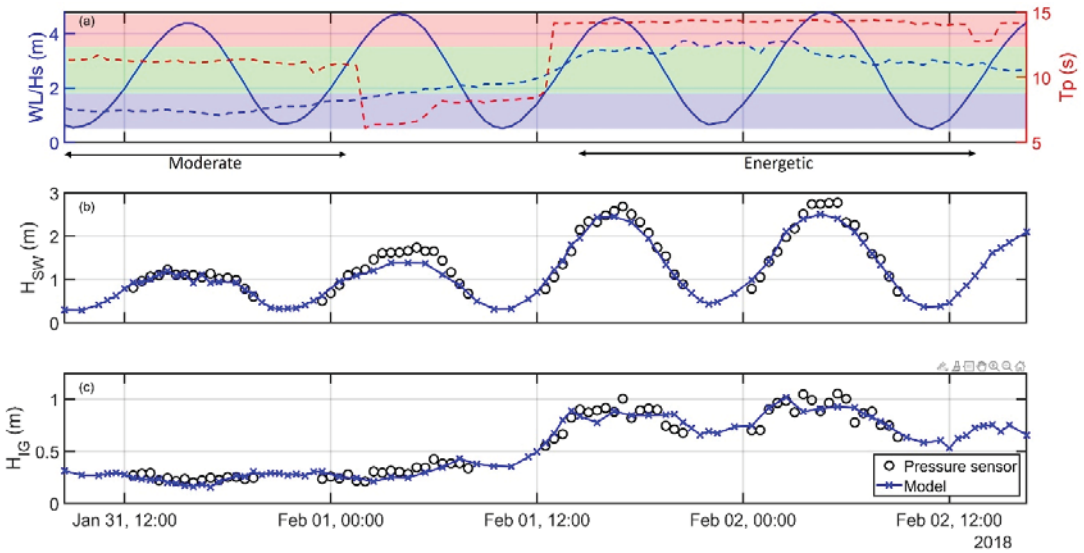

Figure 3. Conditions during the campaign. From top to bottom: water level and offshore Hs/Tp, SW significant wave height, IG significant wave height at a depth +0.3 m. The different classes of conditions are indicated on (a).

The model configuration was thoroughly validated with pressure-derived elevations and video-derived swash measurements in a previous study, which showed satisfying capabilities to reproduce the wave transformations up to the swash zone (PINAULT *et al.*,

2022). An example of the model/observations comparisons is given here at depth +0.3 m above chart datum (CP07 in PINAULT *et al.*, 2022). The model reproduces well the tidally induced variations of H_{SW}, which ranged from about 0.3 m up to 2.7 m. The IG waves temporal evolution is mostly correlated to the increasing offshore wave conditions (rather than to the tidal level). This feature is also well captured by the model. The IG wave heights H_{IG} range from 0.5 m up to 1 m in both model and observations, which is quite significant.

3. Results

3.1 Cross-shore transformation of wave energy

The average energy spectra for the different classes of conditions (Figure 3) are presented on Figure 4. Generally, the high-energy spectra (lower row) exhibit a broader peak saturated with SW energy from about 0.05 Hz up to more than 0.015 Hz. In contrast, the moderately energetic cases show a clear and more delimited peak around 0.08 Hz. When reaching shallow waters, the SW energy decreases due to depth-induced breaking. Simultaneously, an increase of IG energy is noticeable starting around x = 500 m and x = 800 m under moderate and energetic conditions respectively.

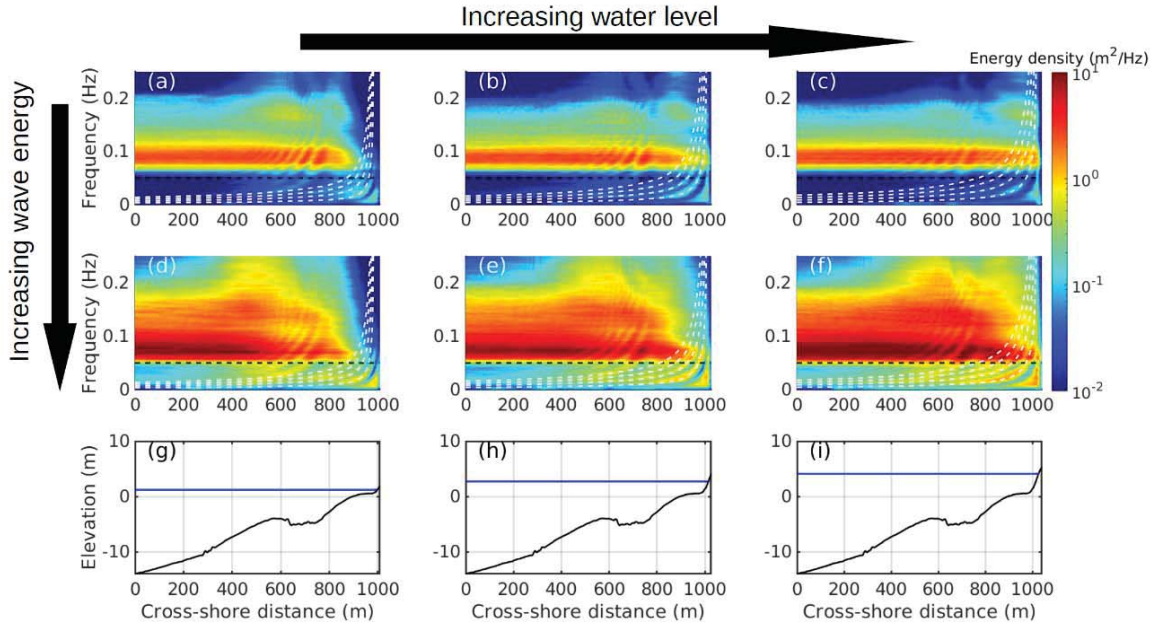

Figure 4. Cross-shore evolution of the wave energy spectrum for each class of conditions. Black dashed line represents the cut-off frequency between SW and IG bands (f_c = 0.05Hz). White dashed lines indicate natural frequencies for a given cross-shore location. The cross-shore bathymetric profile (black) and still water levels (blue) are shown on panels (g)-(i).

The wave spectra also highlight the presence of a standing wave pattern in the IG frequency band close to the shoreline (between x = 800 m and x = 1000 m). Indeed, regions of nearly null energy alternate with regions of high energy, forming a pattern that is typical nodes and anti-nodes alternance (DE BAKKER *et al.*, 2014; BERTIN *et al.*, 2020, MATSUBA *et al.*, 2021). This is corroborated as the anti-node locations observed correspond very well with the analytical locations (white dashed lines on the figure). The presence of a nodal structure appears to be dependent both on tide and wave conditions. At low tide, only the first mode (around 0.02 Hz) is excited, close to the shoreline (around x = 900 m). At mid and high tide, the nodes/anti-nodes are much more visible, especially under energetic conditions.

3.2 IG wave dissipation and reflection

As discussed in the previous paragraph, IG wave reflection at the shoreline is obtained only under certain conditions. The magnitude of the reflection is investigated here by evaluating the reflection coefficient of IG waves R^2 near the shoreline (Figure 5). The reflection coefficient displays a strong tidal modulation, ranging from almost 1 just before high tide (full reflection), down to 0.05 at low tide (almost complete dissipation). This behavior can be explained by the increasing bottom slope from the lowest part of the intertidal zone (β~2-3%), where IG waves are dissipated through breaking, to the upper part of the beach (β~8-10%), where waves are reflected (BERTIN *et al.*, 2020). An interesting feature is the decrease of R^2 at high tide, which seems counter-intuitive at first given the high slope of the foreshore beach. A possible explanation is the presence of a berm at the very top of the foreshore, possibly inducing further dissipation in the swash zone.

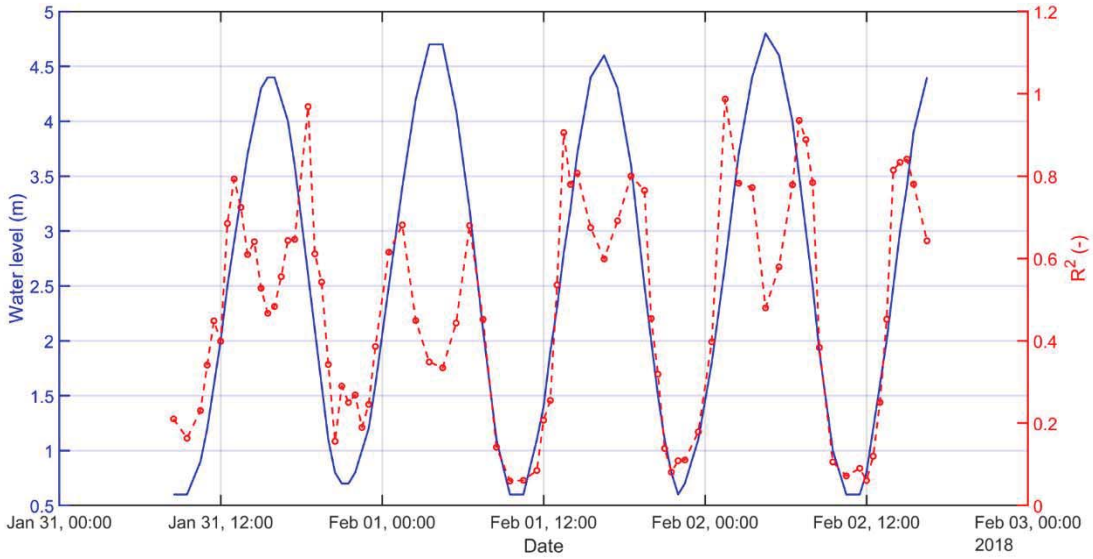

Figure 5. Temporal evolution of the water level (blue) and reflection coefficient R^2 at a depth of 2 m (red).

3.3 Relationship between IG wave and IG swash height

To evaluate the influence of the IG wave dynamics on the swash, the IG swash amplitude at a given frequency is compared to the incoming and outgoing IG wave amplitude on Figure 6. These amplitudes are calculated as $A^{\pm}(f) = \sqrt{\mathrm{d}fE^{\pm}(f)}$ where $E^{\pm}(f)$ is either the incoming/outgoing wave spectrum or the swash spectrum. The IG swash correlates well with the outgoing IG wave amplitude $A_{IG}{}^{-}$ at each frequency, exhibiting a linear relationship with (r^2>0.67). The water level variation, which modulates the entire surf zone and potentially energy dissipation mechanisms, is not seen to affect the relationship, with a regression slope almost constant around 3.5. In contrast, the relationship between $A_{IG}{}^{+}$ and S_{IG} appears more frequency dependent, with decreasing slopes s from 3.61 down to 1.82 as the frequency increases. This suggests that the response of the IG swash to the incoming IG wave decreases with the frequency: the same level of IG wave energy will generate an IG swash of twice the height at 0.01Hz (s=3.6) than at 0.05Hz (s=1.8). Hence, different IG wave components of similar amplitudes will generate different IG swash magnitudes. The linear correlation is also frequency-dependent, as r^2 decreases with increasing frequency, meaning that the swash is better correlated with the incoming IG waves for low frequencies, which is consistent with observations from MATSUBA & SHIMOZONO (2021). This suggests that frequency-dependent IG energy dissipation only affects the shoreward propagating waves.

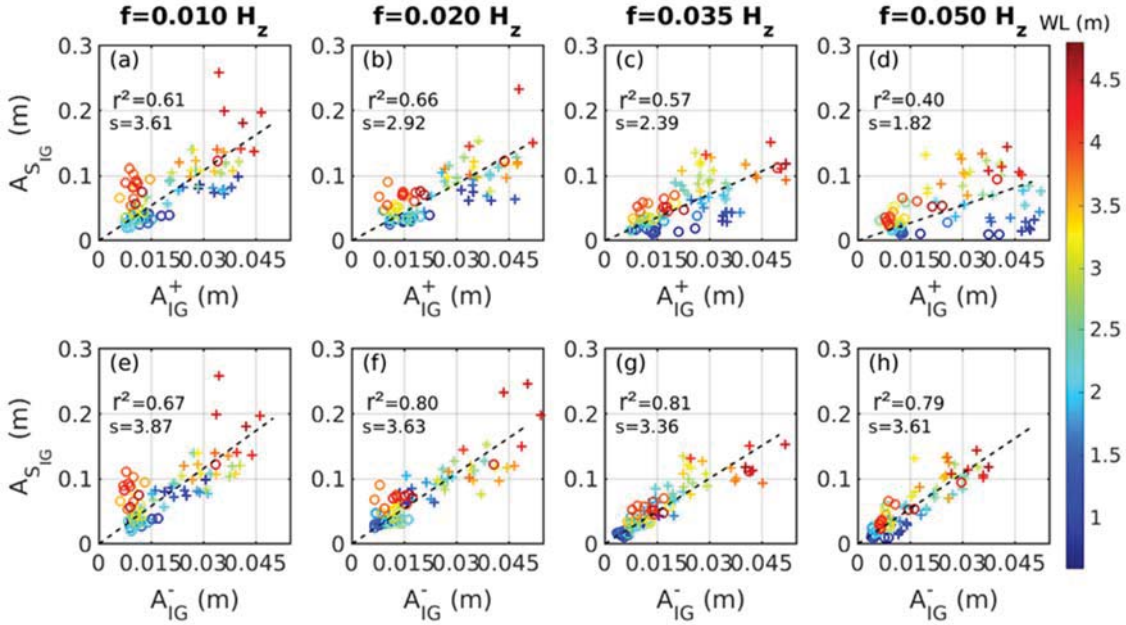

Figure 6. Comparison of the incoming/outgoing IG wave amplitudes measured at a depth of 2 m and IG swash amplitudes for each frequency component. (a)-(d) Incoming IG waves. (e)-(h) Outgoing IG waves. The color scale indicates the water level. Circles and plus signs respectively show the intermediate (Hs <3 m) and energetic (Hs >3 m) offshore wave conditions. r^2 and s respectively indicate the correlation coefficient and the slope of the linear relationship.

4. Conclusions

The IG wave dynamics in the GPB embayment has been explored under varying swell conditions and tidal level using numerical computations. The analysis of the wave spectra shows a nodal structure under conditions that correspond to long waves reflected at the shoreline. The investigation of the reflection coefficient highlights the dissipation of IG energy near the shore. This process appears to be strongly modulated by the tide level, with almost complete dissipation at low tide and strong reflection just before high tide. This behavior is explained by the increase in the active bottom slope: at low tide, the gentle slope allows for IG waves to dissipate through breaking; near high tide, the steep slope favors full IG reflection. These findings are consistent with the IG wave breaking as main dissipation mechanism. Interestingly, the reflection coefficient decreases at full high tide, which suggests that other processes still have a substantial influence. Finally, the results show that the energy dissipation of the IG waves is frequency-dependent, which leads to a variable response of the IG swash to incoming IG waves forcing. The longest incoming waves generated the highest swash due to lower dissipation, with a decreasing linear correlation with increasing frequency. Conversely, the swash height correlation with outgoing waves was similar and high for all frequencies, suggesting no frequency-dependent dissipation for seaward propagating IG waves. These findings shed light on the complex dynamics of IG waves and their interaction with varying wave and tidal conditions.

5. Acknowledgements

This research was carried out under the framework of E2S chair HPC-Waves. The authors acknowledge the related financial support from the I-site program Energy Environ-ment Solutions (E2S), France, the Communauté d'Agglomération Pays Basque (CAPB), France, and the Communauté Région Nouvelle Aquitaine (CRNA), France for the chair HPC-Waves. This research was also supported by the joint laboratory KOSTARISK, which is part of the E2S UPPA program managed by the French National Research Agency (ANR-16-IDEX-0002) and supported by the French Government's "Investissements d'Avenir" (PIA). The joint laboratory KOSTARISK is co-funded by E2S UPPA, the AZTI Foundation and the center Rivages Pro Tech of SUEZ.

6. References

DE BAKKER A.T.M., TISSIER M.F.S., RUESSINK B.G. (2014). *Shoreline dissipation of infragravity waves.* Continental Shelf Research, 72. http://doi.org/10.1016/j.csr.2013.11.013

BERTIN X., MARTINS K., DE BAKKER A., CHATAIGNER T., GUERIN T., COULOMBIER T, DE VIRON O. (2020). *Energy transfers and reflection of infragravity waves at a dissipative beach under storm waves*. Journal of Geophysical Research : Oceans, 125. https://doi.org/10.1029/2019JC015714

INCH K., DAVIDSON M., MASSELINK G., RUSSELL P. (2017). *Observations of nearshore infragravity wave dynamics under high energy swell and wind-wave conditions*. Continental Shelf Research, 138. http://doi.org/10.1016/j.csr.2017.02.010

MATSUBA Y., SHIMOZONO T. (2021). *Analysis of the contributing factors to infragravity swash based on long-term observations*. Coastal Engineering, 169. https://doi.org/10.1016/j.coastaleng.2021.103957

MATSUBA Y., SHIMOZONO T., TAJIMA Y. (2021). *Tidal modulation of infragravity wave dynamics on a reflective barred beach*. Estuarine, Coastal and Shelf Science, 169. http://doi.org/10.1016/j.ecss.2021.107562

MORICHON D., DE SANTIAGO I., DELPEY M., SOMDECOSTE T., CALLENS A., LIQUET B., LIRIA P., ARNOULD P. (2018). *Assessment of flooding hazards at an engineered beach during extreme events : Biarritz, SW France*. Journal of Coastal Research, 85. https://doi.org/10.2112/SI85-161.1

PINAULT J., MORICHON D., DELPEY M., ROEBER, V. (2022). *Field observations and numerical modeling of swash motions at an engineered embayed beach under moderate to energetic conditions*. Estuarine, Coastal and Shelf Science, 279. https://doi.org/10.1016/j.ecss.2022.108143

PINAULT J., MORICHON D., ROEBER, V. (2020). *Estimation of irregular wave runup on intermediate and reflective beaches using a phase-resolving numerical model*. Journal of Marine Science and Engineering, 8, 993. https://doi.org/10.3390/jmse8120993

ROEBER V., CHEUNG K. (2012). *Boussinesq-type model for energetic breaking waves in fringing reef environments*. Coastal Engineering, 70.

ROEBER V., CHEUNG K., KOBAYASHI M. (2010). *Shock-capturing Boussinesq-type model for nearshore wave processes*. Coastal Engineering, vol. 57:407-423.

SHEREMET A., GUZA R. T., ELGAR S., HERBERS T. H. C. (2002). *Observations of nearshore infragravity waves: Seaward and shoreward propagating components*. Journal of geophysical research, 107. https://doi.org/10.1029/2001JC000970

VAN DONGEREN A., BATTJES T., VAN NOORLOOS J., STEENHAUER K., STEENBERGEN G., RENIERS A. (2007). *Shoaling and shoreline dissipation of low-frequency waves*. Journal of geophysical research, 112. https://doi.org/10.1029/2006JC003701